Asian Journal of Chemistry; Vol. 37, No. 12 (2025), 2972-2982
ASIAN JOURNAL OF CHEMISTRY
https://doi.org/10.14233/ajchem.2025.34663

Bioconjugated ZnO Nanoparticles from *Solanum nigrum* Leaves: Monosaccharide Unlocks Potent Antidiabetic and Antioxidant Power

ARCHNA TALWAR[1,*], AVNI NAYYAR[1], SHRUTI ANAND[1], MANAAL ZAHERA[2] and PRACHI SINGH[3]

[1]Department of Chemistry, Isabella Thoburn College, University of Lucknow, Lucknow-226007, India
[2]Department of Biotechnology, Era University, Lucknow-226003, India
[3]Department of Environmental Sciences, Hindu College, University of Delhi, Delhi-110007, India

*Corresponding author: E-mail: archna.05talwar@gmail.com

Received: 8 August 2025 *Accepted*: 23 September 2025 *Published online*: 30 November 2025 AJC-22185

The research focuses on conjugating biogenically synthesized zinc oxide nanoparticles (ZnO NPs) with glucose to analyse the inhibitory potential of ZnO nanoparticles against α-amylase. This study proposes, for the first time, that glucose-modified ZnO NPs may alleviate oxidative stress that hinders the formation of advanced glycation end products (AGEs). ZnO NPs are synthesized by using an aqueous leaf extract of *Solanum nigrum* and characterized using different characterization techniques such as UV-Vis spectroscopy, FESEM, TEM, FTIR, DLS/Zeta and X-ray diffraction. The ZnO NPs were assessed for *in vitro* antioxidant potential, confirming better antioxidant potential of GC-NP (IC_{50} = 45.7 ± 0.18 µg/mL) than UC-NP (IC_{50} = 53.4 ± 0.031 µg/mL). The bio-functionalized ZnO NPs were evaluated for their α-amylase inhibitory activity, showing enhanced inhibition by GC-NP (IC_{50} = 521 ± 0.004 µg/mL) compared to UC-NP (IC_{50} = 530 ± 0.01 µg/mL), attributed to tailored surface interactions. Overall, the study highlights that biofunctionalized ZnO NPs exhibit promising potential as a future drug candidate for targeted drug delivery in diabetes management.

Keywords: Green synthesis, *Solanum nigrum*, Glucose capping, Advanced glycation end products, Oxidative stress.

INTRODUCTION

Diabetes mellitus is a metabolic disorder classified into two types *viz*. (i) Type I (insulin-dependent) and (ii) Type II (insulin-independent). Type II diabetes represents 90-95% of all cases and is strongly linked to sedentary lifestyles and insulin resistance [1,2]. According to the International Diabetes Federation (IDF) Diabetes Atlas (2024), about 10.5% of adults (20-79 years) have diabetes, with 50% unaware of their conditions. IDF projects a 46% rise in global cases by 2045 [3,4]. WHO reports 1.5 million deaths annually, mostly in low- and middle-income countries [5]. Insulin resistance, the main feature of diabetes, is associated with oxidative stress. The formation of advanced glycation end products (AGEs) in diabetics can bind to RAGE receptors, triggering inflammatory pathways (NF-κβ) and generating reactive oxygen species (ROS) [6]. This oxidative stress alters glucose transporters like GLUT4, impairing glucose uptake and promoting insulin resistance [7,8]. Treatments include insulin therapy and oral drugs such as biguanides, thiazolidinediones and sulfonylureas. Sodium-glucose co-transporter 2 (SGLT2) inhibitors like dapagliflozin and empagliflozin also lower blood glucose and provide cardiovascular benefits [9]. However, these treatments may cause side effects such as nausea and edema, emphasizing the need to maintain glucose homeostasis without chronic complications [10].

The bioactive compounds in *Solanum nigrum* (Solanaceae) leaves exhibit antidiabetic activity and may serve as natural agents for blood glucose regulation. However, their poor solubility and bioavailability limit therapeutic use. Integrating these extracts with nanotechnology enhances their delivery within biological systems [11,12]. The diversity of plant metabolites and their scalability make them attractive for nanoparticle synthesis [13]. Phytoconstituents in plants act as reducing and stabilizing agents and variations in extract concentration can influence nanoparticle morphology [14]. The biosynthetic approach avoids toxic chemicals and finds applications in product manufacturing, disease diagnosis and environmental remediation [15]. *S. nigrum* is rich in flavonoids, anthocyanins, tannins and steroidal derivatives, with antioxidant and pharmacological

activities [16]. These metabolites reduce oxidative stress, lowering risks of diabetes, cardiovascular diseases as well as cancer.

Among metal oxides, zinc oxide (ZnO) has gained significant biomedical interest due to its biodegradability, low toxicity and cost-effectiveness [17]. It is recognized as a GRAS (Generally Recognized as Safe) material by the US FDA [18]. The morphology and properties of ZnO nanoparticles vary with plant extract concentration and synthesis conditions, influencing their biological activity [19]. The biological significance of zinc lies in its ability to bind proteins and enzymes, playing a vital role in insulin synthesis, storage and secretion by enhancing PI3K activity, stimulating insulin receptor phosphorylation and inhibiting glycogen synthase kinase [20]. It also supports insulin activity through carboxypeptidases and facilitates intracellular insulin receptor trafficking [21,22]. Adequate zinc levels are thus essential for diabetes prevention. ZnO nanoparticles further inhibit α-glucosidase and α-amylase by blocking their active sites, causing non-competitive and competitive inhibition that reduces enzyme catalytic efficiency [23,24].

This study focuses on conjugating biogenically synthesized ZnO NPs with a hydrophilic moiety, *i.e.* glucose and its inhibitory effect on α-amylase. It may be hypothesized that fabricating nanoparticles with glucose reduces oxidative stress by lowering the accumulation of AGEs due to the interruption of the glycoxidation process. The capping with glucose may improve the dispersion of ZnO NPs and increase their surface area, allowing them to interact with the binding sites of α-amylase. Zinc ions may stabilize proteins, inhibit the activity of glycation-promoting enzymes and neutralize dicarbonyl compounds (*e.g.* methylglyoxal) to hinder their participation in AGE formation [25]. Thus, coating with a hydrophilic moiety can increase the circulation half-life of nanoparticles within the biological system and reduce agglomeration [26]. This may provide an avenue for loading a drug molecule onto a nanoparticle by avoiding unwanted toxicity. Thus, coating nanoparticles with a hydrophilic moiety can extend their circulation half-life within the biological system and reduce agglomeration [27]. This may provide a promising strategy for loading a drug molecule onto a nanoparticle by avoiding unwanted toxicity.

EXPERIMENTAL

Zinc acetate dihydrate and D-glucose (anhydrous) were bought from Qualigens, Thermo Fisher Scientific India Pvt. Ltd., Mumbai, India.

Sample collection: The fresh *Solanum nigrum* leaves were collected from the garden of Isabella Thoburn College (26.8563ºN, 80.9499ºE) Lucknow, India. The plant specimen was authenticated by the herbarium of the National Botanical Research Institute (NBRI),

Preparation of aqueous leaf extract: The leaves were thoroughly washed with distilled water to remove the contaminants and dried to eliminate moisture. Approximately 15 g of dried, powdered leaves were soaked in 200 mL of Milli-Q water. The mixture was heated in a water bath at 60 ºC for 30 min and allowed to cool. The solution was left overnight and then filtered using Whatman filter paper 1. The resulting filtrate was stored at 4 ºC.

Biogenic synthesis of ZnO NPs: For the synthesis of uncapped ZnO NPs (UC-ZnO NPs), 50 mL of leaf extract and 5 g of $Zn(CH_3COO)_2 \cdot 2H_2O$ were mixed and stirred on a magnetic stirrer at 70 ºC for 3 h, centrifuged at 3000 rpm for 20 min, thrice. The sample was then dried in a hot air oven at 80 ºC and subsequently heated in a muffle furnace at 400 ºC for 2 h, followed by grinding the sample into a fine powder. The synthesis of glucose-capped ZnO NPs (GC-ZnO NPs) was carried out by mixing 35 mL of plant extract with 3.5 g of $Zn(CH_3COO)_2 \cdot 2H_2O$ at 70 ºC using a magnetic stirrer for 1 h. After the initial stirring, 1.76 g of glucose was added and stirred for 2 h.

The percentage yield of UC-ZnO NPs obtained after synthesis was approximately 2%, while that of GC-ZnO NPs was around 3%. The variation in yield can be attributed to the differences in the initial mass of precursor zinc ions used during the reaction. The synthesis procedure was repeated multiple times to confirm reproducibility. The relatively low yield may be due to factors such as material loss during repeated centrifugation, decomposition of organic matter during calcination, and other process-related losses.

Characterization: The biosynthesized ZnO NPs were characterized using UV-visible spectroscopy, field-emission scanning electron microscopy (FESEM), transmission electron microscopy (TEM), dynamic light scattering and Fourier transform infrared spectroscopy (FT-IR). The UV-visible absorbance of the ZnO nanoparticles was measured using a Shimadzu 1601 spectrophotometer (Japan). The surface morphology and shape of ZnO nanoparticles were analyzed using the JEOL-JSM 7610f instrument (Japan). Transmission electron microscopy (TECNAI 20G2, Thermo-Fischer) was used to examine the agglomeration in the metallic nanoparticles. Malvern Zeta Sizer (U.K.) determined the size distribution and ζ-potential of the synthesized nanoparticles. The identification of various phytoconstituents responsible for the reduction of ZnO NPs was carried out by Bruker Alpha II 210966 FT-IR spectrometer (USA) in the range of 3200-400 cm^{-1}. The X-ray diffraction pattern was obtained within a range of 5º to 80º using Cu*K*α radiation with a wavelength of 1.54059 Å.

***In vitro* antioxidant activity:** The ability of secondary metabolites to inactivate free radical species is responsible for their antioxidant nature. The bioactive compounds neutralize free radicals of DPPH by donating hydrogen atoms or transferring electrons, resulting in a colour change from purple to yellow. The extent of colour change reflects the scavenging activity of bioactive components [28]. The free radical scavenging activity of UC-ZnO NPs, GC-ZnO NPs was evaluated using ascorbic acid as a standard. The stable radical 2,2-diphenyl-1-picrylhydrazyl (DPPH), known for its purple colour and a distinct absorption peak at 515 nm, served as an indicator. To 1 mL of 0.1 mM methanolic solution of DPPH, different concentrations of 30, 40, 50, 60 and 80 μg/mL of UC-ZnO NPs, GC-ZnO NPs were added. After 30 min of incubation in dark, the absorbance of each test sample was recorded at 515 nm using a UV-Vis spectrophotometer. The free radical scavenging activity of the biosynthesized ZnO NPs was compared with that of the standard and the percentage of

scavenged free radicals was calculated using the following formula:

$$\text{Scavenging activity (\%)} = \frac{\text{Abs}_{\text{control}} - \text{Abs}_{\text{sample}}}{\text{Abs}_{\text{control}}} \times 100$$

α-Amylase inhibition assay: The inhibitory activity of α-amylase was assessed by measuring the amount of reducing sugar released under the assay conditions [21]. The *in vitro* α-amylase inhibition assay was carried out using the DNSA method for UC-ZnO NPs, GC-ZnO NPs and metformin. A stock solution of 1 mg/mL of both nanoparticles was prepared by dissolving 10 mg of nanoparticles in 10 mL of DMSO. Different volumes of ZnO nanoparticles ranging from 200 µg/mL, 400 µg/mL, 600 µg/mL, 800 µg/mL and 1000 µg/mL were diluted with PBS (pH 6.9) to make 1 mL of solution, which were pre-incubated with 100 µL α-amylase for 30 min at 37 ºC. In a reaction mixture, 100 µL of 1 % starch solution was added to the test tubes and incubated for 30 min at 37 ºC. To quench the reaction, 200 µL of DNSA reagent (3,5-dinitrosalicylic acid) was added to the reaction mixture. The resulting solution was kept in a boiling water bath for 5 min at 100 ºC and the absorbance value was measured at a wavelength of 540 nm by a UV-spectrophotometer. An antidiabetic drug, metformin, was used as a control. The percentage inhibition of α-amylase was calculated using the following formula:

$$\text{Inhibition (\%)} = \frac{\text{Abs}_{\text{control}} - \text{Abs}_{\text{sample}}}{\text{Abs}_{\text{control}}} \times 100$$

Statistical analysis: All statistical analyses were conducted using OriginPro 2024b to ensure the reliability of the results. Statistical significance was considered at a threshold of $p < 0.05$ and the experiments were performed in triplicate. The graphs were plotted using Microsoft Excel.

RESULTS AND DISCUSSION

The biosynthesis of nanoparticles is an energy-efficient process and avoids the use of hazardous chemicals [22]. The study describes the synthesis of uncapped and glucose-capped zinc oxide nanoparticles from an aqueous extract of *Solanum nigrum* leaves. The secondary metabolites are thought to function as reducing agents, facilitating the conversion of zinc acetate dihydrate into ZnO NPs [29]. The size and stability of nanostructures are governed by these redox reactions during the interaction of the phytoconstituents with the metal ions [23,24]. The attack of metal ions on –OH, -COOH functional groups of secondary metabolites favours the formation of hydrophilic surfaces suitable for the growth of nanoparticles [30] (Fig. 1). Moreover, the amount of the plant extract influences the redox process and the role of the capping agent becomes crucial, as it provides stability in preventing the agglomeration and brings stability to the nanoparticles through steric, electrostatic or electrosteric interactions [31]. Moreover, the surface capping of the nanoparticles enhances biocompatibility and reduces toxicity in living cells [32]. Hence, glucose has been reported as a suitable coating agent for nanoparticles, as it improves their target efficiency through polar interactions with surface receptors [33]. Moreover, surface tailoring may lead to improved dispersion and the formation of a hydrophilic shell by promoting surface interactions with biological media [34].

ZnO nanoparticles decorated with phytocomponents inhibit α-amylase by competitively or non-competitively blocking its active sites, reducing the hydrolysis of complex carbohydrates into simple sugars and lowering postprandial hyperglycemia [35]. Without inhibitors, elevated glucose levels accelerate ROS formation, disrupting redox balance and causing oxidative stress [36]. Hyperglycemia also strains mitochondria, generating superoxide and free radicals, contributing to diabetic complications such as nephropathy, retinopathy and cardiovascular diseases [37]. High glucose promotes non-enzymatic glycation, forming advanced glycation end products (AGEs) [38]. Reactive carbonyl species like glyoxal and methylglyoxal modify amino acids and activate AGE receptors (RAGE), triggering pathways such as NF-κβ that promote inflammation [39,40]. Glucose-capped ZnO NPs may bind reactive carbonyl species, inhibit AGE formation, and modulate RAGE expres-

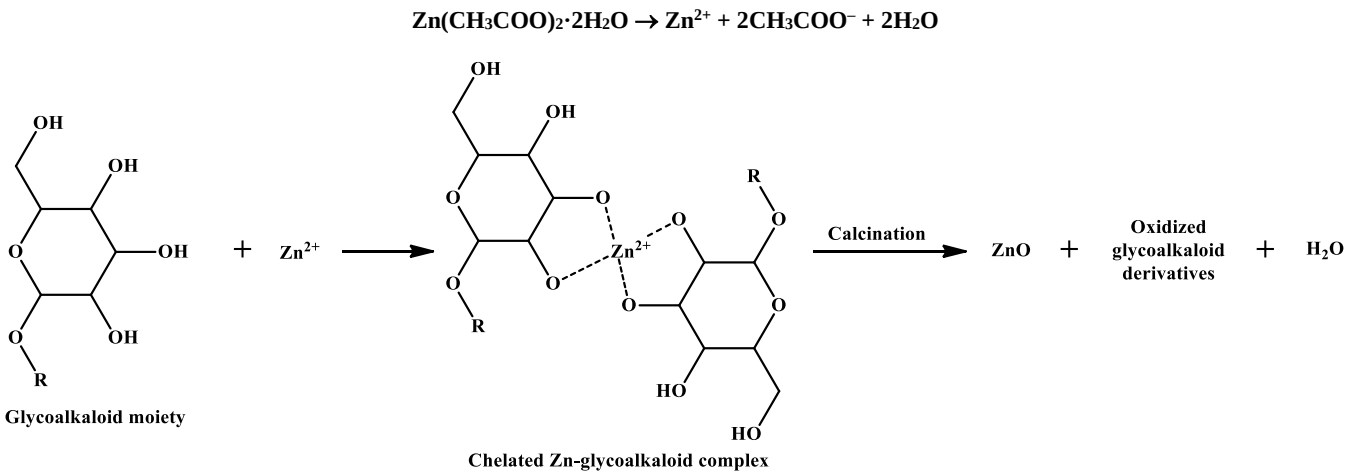

In the presence of glucose, ZnO nanoparticles interact with glucose molecules to prevent agglomeration

ZnO + Glucose → [ZnO]-----OH + Gluconic acid + H_2O

Fig. 1. Proposed mechanism of formation of ZnO nanoparticles

sion. Zinc ions from ZnO NPs act as cofactors for enzymes such as catalase and superoxide dismutase, neutralizing free radicals, maintaining protein structure and reducing glycation, thereby enhancing targeted therapeutic effects.

UV-Visible studies: The UV absorption peaks of GC ZnO-NPs and UC ZnO-NPs were observed at 224 nm and 228 nm, respectively (Fig. 2a-b). The absorption spectrum of GC ZnO-NPs shifted to a lower wavelength than that of UC ZnO-NPs due to the large excitation binding energy, which is attributed to the smaller size of the nanoparticles [41,42]. The band gap corresponding to the reported wavelength of GC ZnO-NPs and UC ZnO-NPs was calculated using Tauc's plot and is obtained at 5.34 eV and 5.23 eV, respectively (Fig. 3a-b). The synthesis method and surface chemistry play a critical role in determining the extent of the blue shift. In the given study, ZnO nanoparticles were synthesized hydrothermally and literature has reported that hydrothermally synthesized nanoparticles show low absorption peaks due to quantum effects [43]. The phytochemicals present in the leaf extract can act as electron donors or acceptors, thereby modifying the surface chemistry of ZnO nanoparticles [44]. Doping these biogenic nanoparticles with glucose passivates their surface by intense hydrogen bonding and other electronic effects, contributing to a blue shift in the spectra [45]. Furthermore, glucose with multiple binding sites can reduce trap densities, consequently alter the magnetic and electronic environment, resulting in a broader band gap [46]. The wide band gap may also be attributed to electronic transitions from $\delta \rightarrow n$ or $\pi \rightarrow \pi^*$ within the ZnO nanosystem [47]. This is in accordance with the reported studies that doping with glucose and other organic agents can significantly modify the optoelectronic properties of the ZnO NPs [48,49]. It has also been reported that ZnO nanorods with diameters up to 180 nm can exhibit blue shifts due to surface resonance effects [50]. In the present work, a well-defined, sharp peak indicates that the nanoparticles are monodisperse, stable and less agglomerated.

Morphological studies: FESEM studies illustrate the surface images and size distribution of GC ZnO-NPs and UC

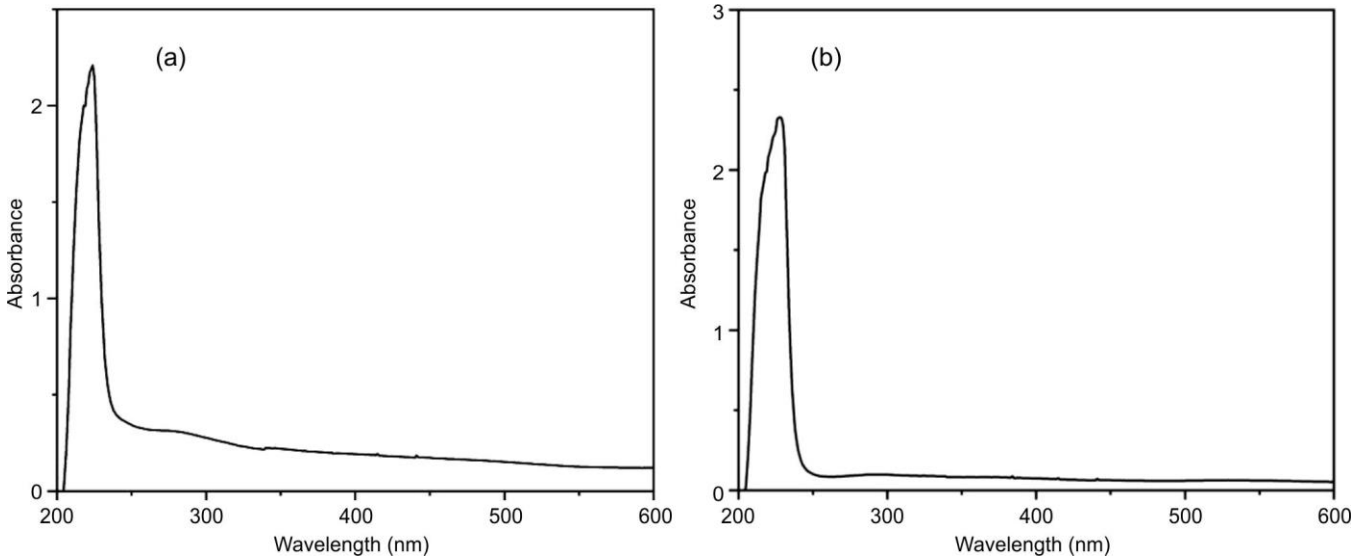

Fig. 2. UV-visible absorption peak (a) GC ZnO-NPs and (b) UC ZnO-NPs

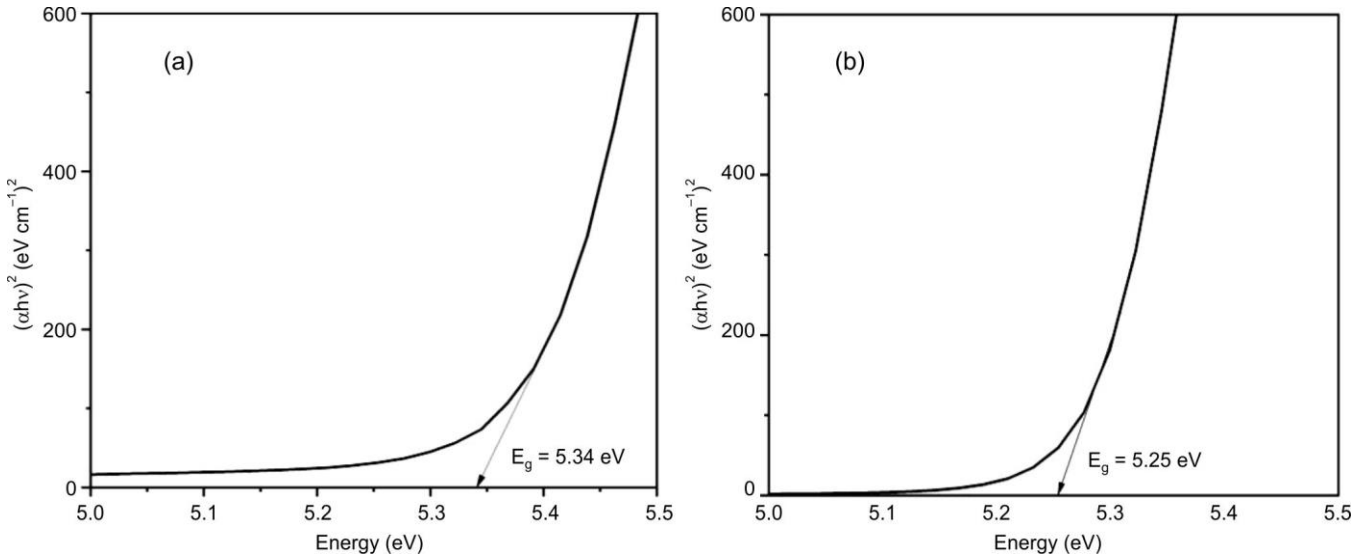

Fig. 3. Tauc plot (a) GC ZnO-NPs and (b) UC ZnO-NPs

ZnO-NPs (Fig. 4). The FESEM images of GC ZnO-NPs show an average size of 46 nm, as compared to UC ZnO-NPs, which shows an average size of 60 nm (Fig. 5). The highly magnified image depicts the ZnO NPs in their agglomerated form, suggesting the encapsulation of plant extracts with the metal ion [51]. The nanoparticles in GC ZnO-NPs appear smaller in size and have less agglomeration than the FESEM images of UC ZnO-NPs. This suggests and confirms the effect of glucose as

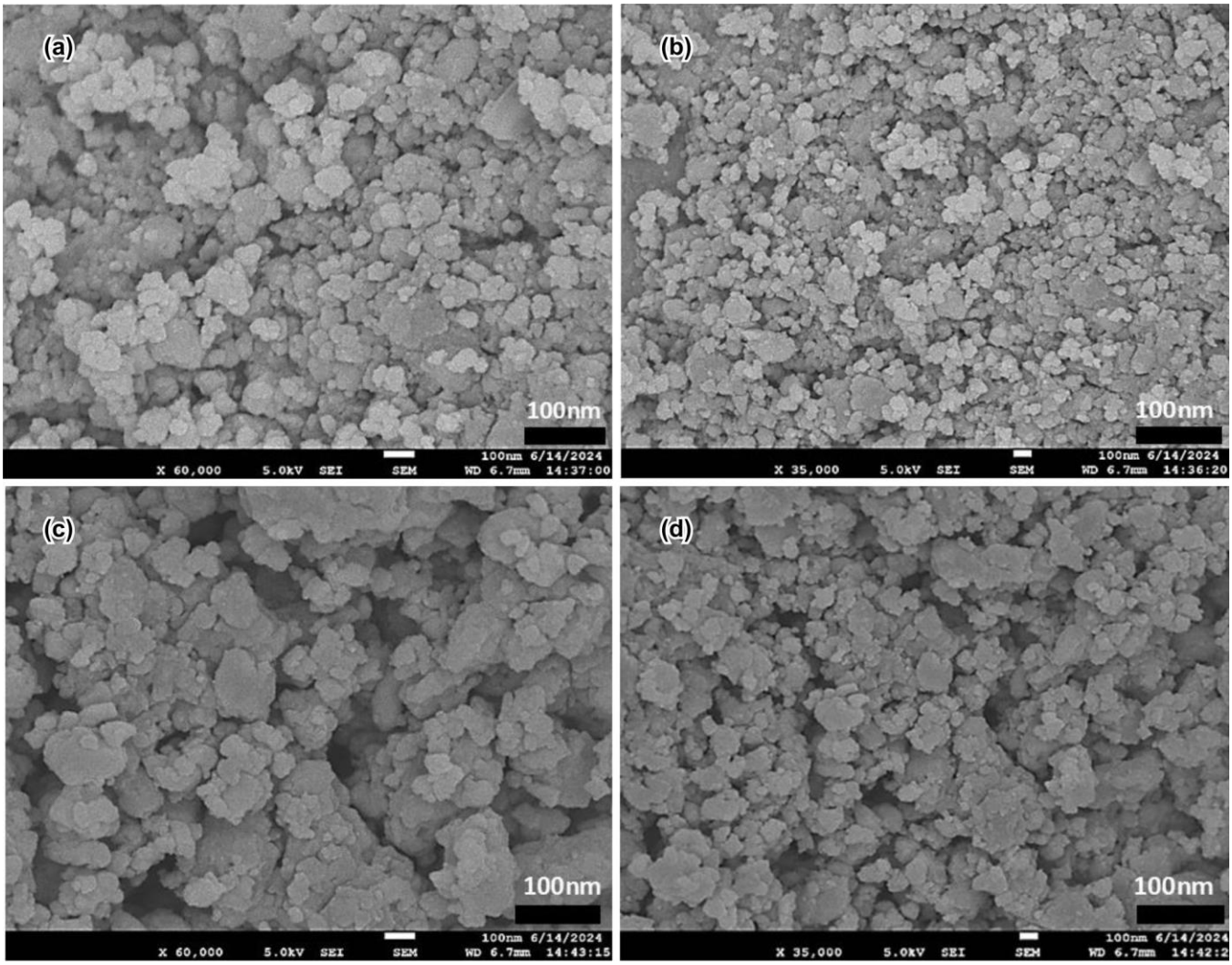

Fig. 4. FESEM of GC ZnO-NPs (a) X60,000 (b) X35,000; FESEM of UC ZnO-NPs (c) X60,000 and (d) X35,000

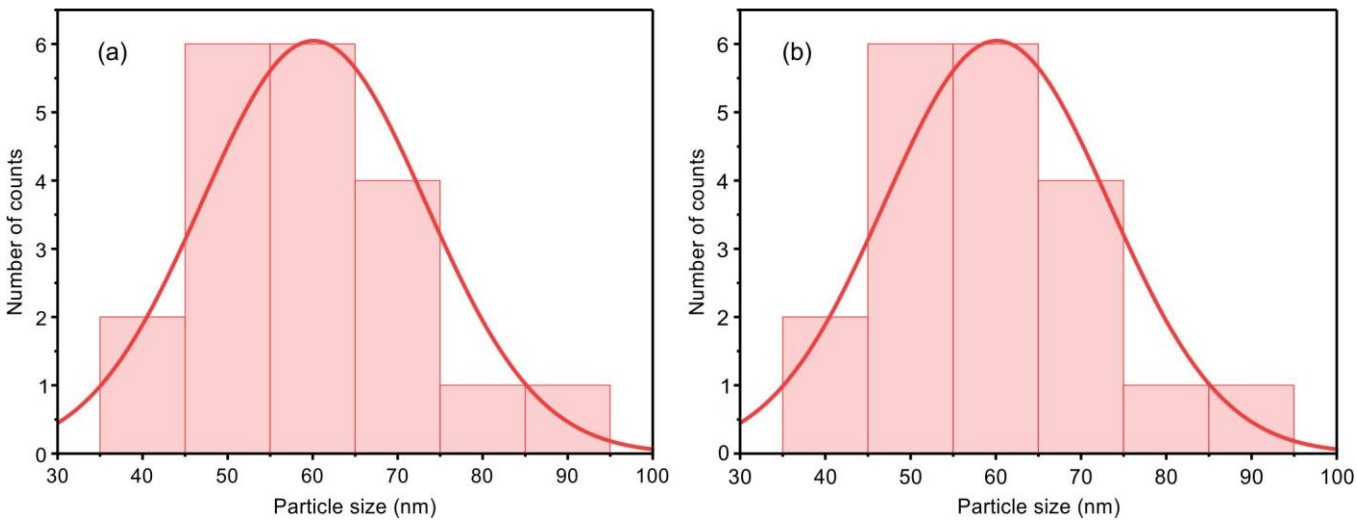

Fig. 5. Nanoparticle size histograms (a) GC ZnO-NPs [average size 46 nm] and (b) UC ZnO-NPs [average size 60 nm]

a capping agent in GC ZnO-NPs, limiting agglomeration and ensuring colloidal stability as compared to UC ZnO-NPs without a capping agent [21,52].

The elemental composition of the biogenically synthesized ZnO NPs was analyzed by energy dispersive X-ray diffraction (EDX) studies. The studies suggest that emission peaks for uncapped ZnO nanoparticles lie between 1 and 10 keV [53,54]. The spectrum of GC ZnO-NPs was observed at 1 keV, 8.6 keV and 9.6 keV, aligning well with previous reports [55] (Fig. 6). A single peak for oxygen was observed at 0.5 keV, which confirms the formation of ZnO NPs [56]. A typical carbon peak at 0.3 keV is likely due to the organic capping agent (glucose). The emission peaks of phosphorus and aluminium indicate the presence of trace elements during the synthesis process. Hence, the spectrum analysis reveals successful capping of glucose on ZnO NPs.

The TEM images demonstrate that ZnO NPs are spherical to irregular. The particles are agglomerated, a common phenomenon in oxide particles [57] (Fig. 7a). The uncapped ZnO-NPs exhibit extensive agglomeration, indicating that the coating of nanoparticles reduces their uncontrolled growth

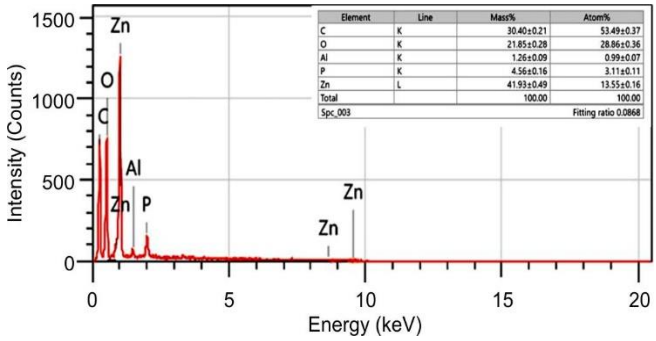

Fig. 6. Energy dispersive X-ray diffraction spectrum of GC ZnO-NPs

and clustering (Fig. 7b). The different rings observed in the selected area electron diffraction pattern (SAED) suggest that the nanoparticles are crystalline with a preferential distribution [58] (Fig. 7b-d).

DLS/zeta potential: The average size and surface charge of the synthesized nanoparticles were determined using dynamic light scattering (DLS) and zeta potential measurements, respectively (Fig. 8). The average diameter of GC ZnO-NPs from

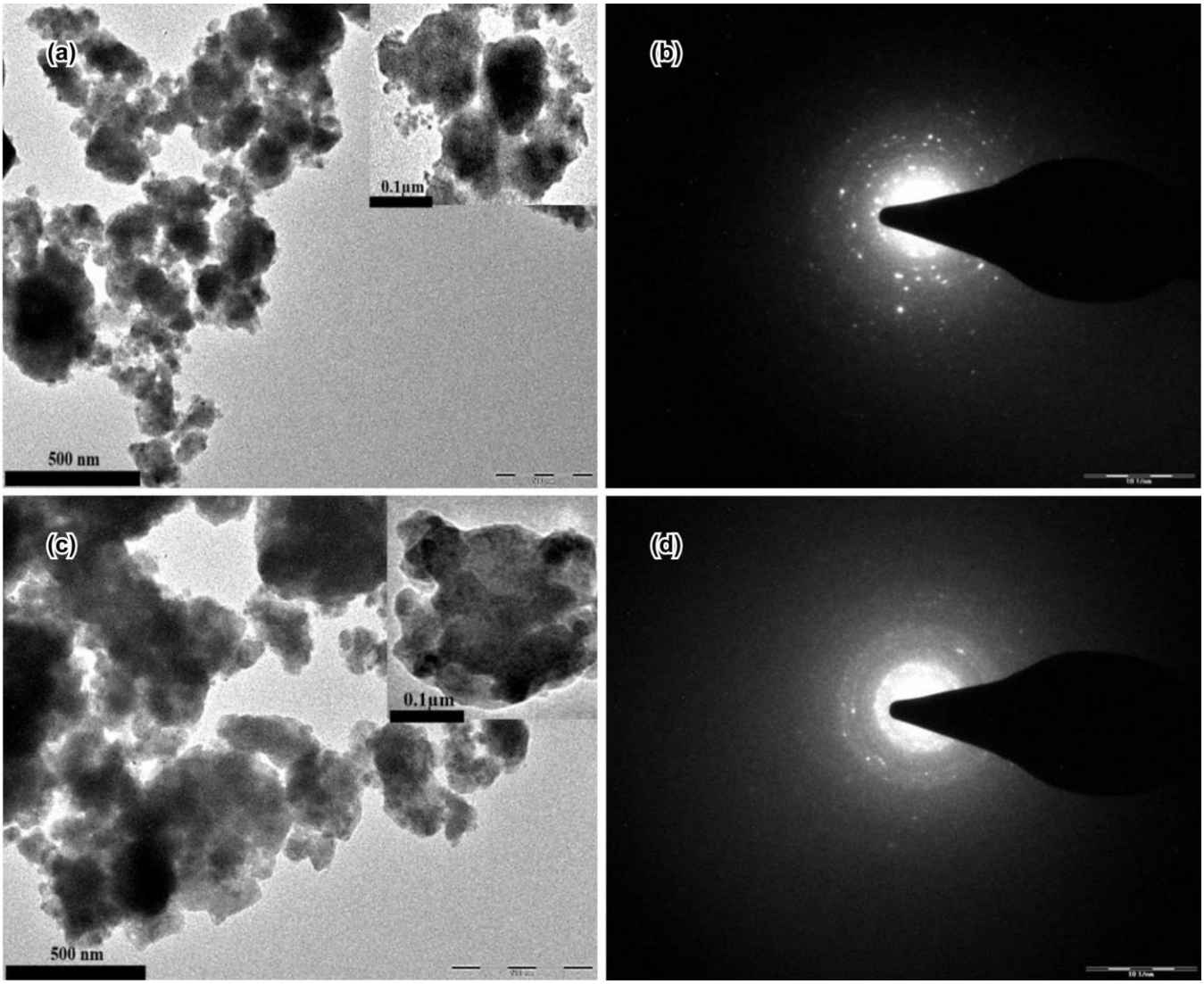

Fig. 7. (a) TEM of GC ZnO-NPs, (b) SAED of GC ZnO-NPs, (c) TEM of UC ZnO-NPs and (d) SAED of UC ZnO-NPs

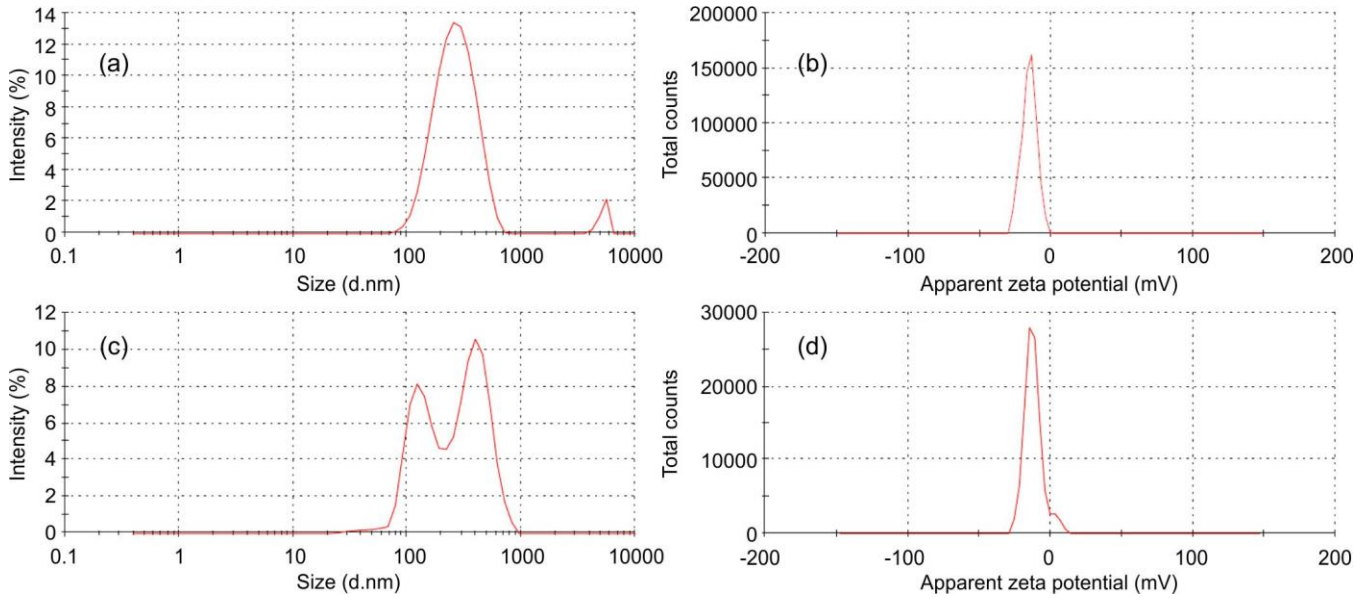

Fig. 8. (a,b) Size distribution and zeta potential of GC ZnO-NPs; (c,d) Size distribution and zeta potential of UC ZnO-NPs

DLS was found to be 270 nm (mean of single peak ~90 nm). This is larger than the size estimated from the SEM analysis. Similarly, the average diameter of UC ZnO-NPs was found to be 411 nm (mean of single peak ~137 nm). The variation in size may be due to the formation of hydration layers and the bioorganic components surrounding the core of the nanoparticles [59-61]. The Z-average size calculated by the DLS technique reflects the hypothetical size of nanoparticles surrounded by solvation shells and stabilizing molecules in solution [62,63]. In case of GC ZnO-NPs, the particles are stabilized by both steric and electronic factors, resulting in a more uniform distribution. Conversely, UC ZnO-NPs lacks stabilization, causing the particles to cluster into larger agglomerates, resulting in a larger apparent size compared to the core dimensions. It can be said that the particle size obtained from DLS analysis differs from SEM studies, as SEM measures the physical core size of the nanoparticles under dry and high vacuum conditions, whereas DLS measures the size of nanoparticles that dynamically diffuse in solution [62,64].

The negative zeta potential of GC ZnO-NPs, -15 mV, confirms that the biomolecules encapsulating metal ions consist of negatively charged groups [54,65]. In contrast, the zeta potential for UC ZnO-NPs was recorded at -12 mV. However, the reported zeta potential values fall within the moderate stability range. Previous studies have reported ZnO nanoparticles with zeta potentials of ± 15 to 20 mV and were described as stable with anti-agglomeration properties [66,67]. This study focuses on the stability of capped nanoparticles. In present *in vitro* analysis, the nanoparticles remained well-dispersed, producing significant results. Functionalization with therapeutic molecules or drugs may further enhance their stability and biocompatibility under physiological conditions [68]. The homogeneity of the nanoparticles in aqueous solution was assessed using the polydispersity index (PDI). GC ZnO-NPs exhibited a PDI of 0.34, indicating higher homogeneity compared to UC ZnO-NPs, which were more heterogeneous with a PDI of 0.48 [69-71].

FT-IR spectral studies: The detection of various functional groups contributing to the stabilization of the ZnO NPs was carried out by FT-IR spectroscopy (Fig. 9). The FT-IR spectrum of GC ZnO-NPs showed peaks at 3431 cm^{-1}, 2925 cm^{-1}, 2338 cm^{-1}, 1495 cm^{-1}, 1413 cm^{-1} and 1048 cm^{-1}, which closely correspond to the peaks of different phytoconstituents of dried *S. nigrum* leaf extract [72]. The synthesized ZnO NPs show a broad absorption band at 3431 cm^{-1} due to O-H stretching vibrations in polyphenolic compounds [73]. Another peak at 2925 cm^{-1} of GC ZnO-NPs is attributed to the aldehydic C-H stretching vibrations or asymmetric vibration of C-H associated with glucose [74,75]. The peak at 2859 cm^{-1} (UC ZnO-NPs) corresponds to the stretching vibration of C-H of the alkane group [76]. The peak at 2338 cm^{-1} (GC ZnO-NPs) and the peak at 1556 cm^{-1} (UC ZnO-NPs) correspond to the –N-H stretching of amide in proteins [77,78]. The absorption peak at 1495 cm^{-1} of GC ZnO-NPs and 1455 cm^{-1} of UC ZnO-NPs (1510-1450 cm^{-1}) can be related to C=C-C aromatic ring stretching vibrations or stretching of N-H vibration [72,78]. Another peak at 1413 cm^{-1} may be assigned to the C-O stretching of alcohols, carboxylic acids, ethers and anhydrides, or the symmetric stretching of carboxyl groups in amino acid residues [61,79]. Also, this peak at 1413 cm^{-1} might be due to the various atomic groups containing a hydrogen atom associated with glucose [80]. The ZnO stretching vibration is detected within the range of 600-400 cm^{-1} [81]. The peak at 1048 cm^{-1} is commonly observed in both UC ZnO-NPs and GC ZnO-NPs [69]. Notably, the peak specific to glucose is absent in UC ZnO-NPs. Therefore, FT-IR spectral analyses reveal that different phytoconstituents are associated with the metal ion and assist in the synthesis of ZnO NPs.

X-ray diffraction (XRD) analysis: The XRD patterns of GC ZnO-NPs and UC ZnO-NPs revealed diffraction peaks at 2θ values (Fig. 10) corresponding to (hkl) at (100), (002), (101) and (102). These peaks correspond to a hexagonal wurtzite structure of ZnO, according to JC-PDS card no. 36-1451 [82]. The average crystallite size of the nanoparticles was determined using Scherrer's formula:

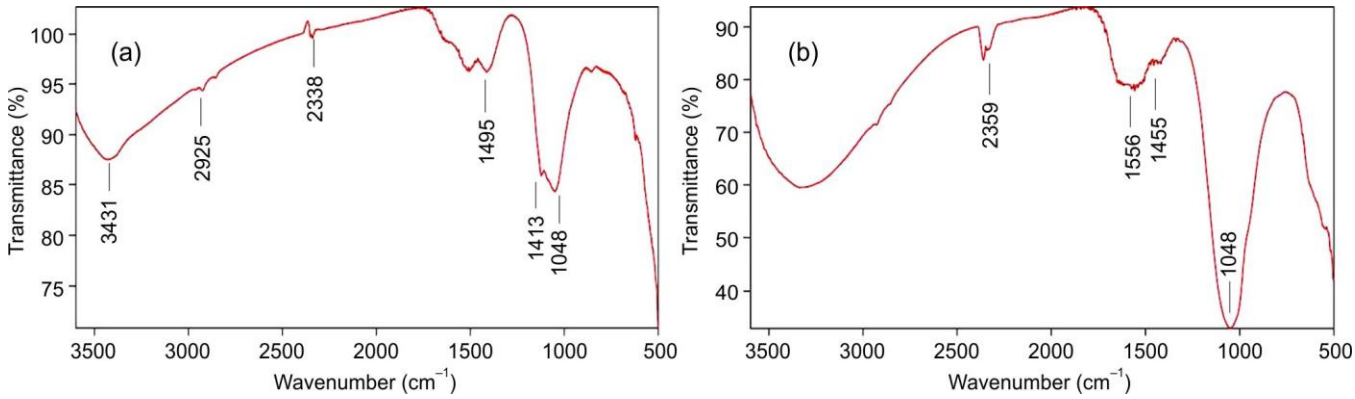

Fig. 9. FT-IR spectra (a) GC ZnO-NPs and (b) UC ZnO-NPs

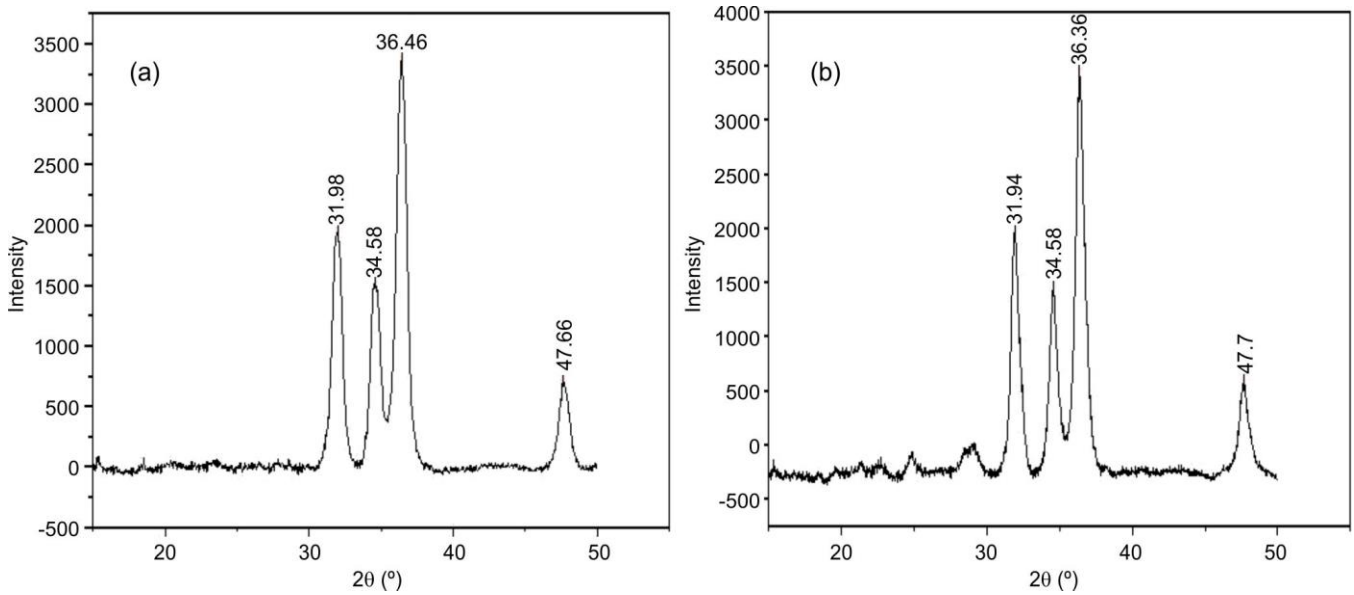

Fig. 10. X-ray diffraction pattern (a) GC ZnO-NPs and (b) UC ZnO-NPs

$$D = \frac{0.89\lambda}{\beta \cos\theta}$$

where 0.89 = Scherrer's constant; β = full width at half maximum (FWHM); λ = X-ray wavelength (1.5406 Å) and θ = Bragg's angle of diffraction [83]. The average crystallite size of GC ZnO-NPs and UC ZnO-NPs was reported at 9.95 nm and 10.83 nm, respectively.

The reported crystallite size significantly differs from the SEM size, as SEM analysis reveals the architectural morphology of the crystallites clustered together, while XRD determines primary nanocrystalline domains within the nanocomposition [53,66]. Thus, the comparative data (Table-1) obtained from the characterization results revealed that encapsulating nanoparticles with a biocompatible moiety like glucose enhances the stability of ZnO NPs and offers avenues for various biomedical applications.

***In vitro* antioxidant activity:** The antioxidant potential of *S. nigrum* leaves has been extensively reported in the literature [84]. The free radical scavenging activity results revealed that the biosynthesized ZnO NPs exhibited dose-dependent antioxidant activity. However, their scavenging potential was comparatively lower than that of the standard. The highest

TABLE-1
COMPARATIVE STUDY OF REPORTED VALUES OF CHARACTERIZATION TECHNIQUES OF GC ZnO-NPs AND UC ZnO-NPs

Characterization techniques	Nanoparticles	Reported values
UV-Vis spectroscopy	GC ZnO-NPs	224 nm
	UC ZnO-NPs	228 nm
FE-SEM	GC ZnO-NPs	46 nm
	UC ZnO-NPs	60 nm
Dynamic light scattering	GC ZnO-NPs	270 nm
	UC ZnO-NPs	411 nm
Zeta potential	GC ZnO-NPs	-15 mV
	UC ZnO-NPs	-12 mV
Polydispersity index	GC ZnO-NPs	0.34
	UC ZnO-NPs	0.48
X-ray diffraction	GC ZnO-NPs	9.95 nm
	UC ZnO-NPs	10.83 nm

DPPH activity was recorded for both ZnO NPs and the standard at 80 μg/mL. The % inhibition for GC ZnO-NPs and UC ZnO-NPs were observed at 71% (IC_{50} = 45.7 ± 0.18 μg/mL) and 58% (IC_{50} = 53.4 ± 0.031 μg/mL), respectively, as compared

to 81% (IC_{50} = 39 ± 0.02 µg/mL) for ascorbic acid. The electron-donating ability of ZnO NPs to DPPH radical is responsible for their antioxidant property. Notably, GC ZnO-NPs exhibited a relatively higher antioxidant activity than UC ZnO-NPs, confirming the presence of a negative charge, as indicated by the zeta potential results. The enhanced interaction between negatively charged bioactive compounds and positively charged metal ions in GC ZnO-NPs increased the antioxidant potential as compared to UC ZnO-NPs [85] (Fig. 11, Table-2).

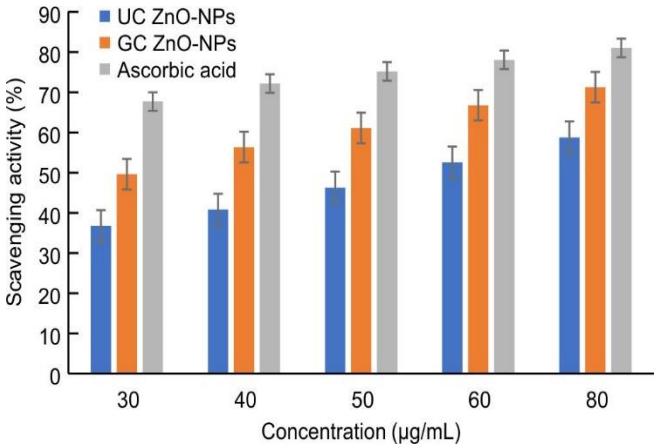

Fig. 11. Antioxidant assay of ZnO nanoparticles and ascorbic acid

TABLE-2
In vitro ANTIOXIDANT ACTIVITY OF
ZnO NANOPARTICLES AND ASCORBIC ACID

Samples	Maximum % inhibition	IC_{50} (µg/mL)
GC ZnO-NPs	71	45.7 ± 0.180
UC ZnO-NPs	58	53.4 ± 0.031
Ascorbic acid	81	39.0 ± 0.020

*Data are IC_{50} ± SD (Standard deviation).

α-Amylase inhibition assay: A significant increase in the inhibitory activity of ZnO NPs and metformin was observed against α-amylase with increasing concentrations of the nanoparticles and control. The IC_{50} for GC ZnO-NPs, UC ZnO-NPs and control were determined at 521 ± 0.004 µg/mL, 530 ± 0.01 µg/mL and 502 ± 0.01 µg/mL, respectively. The results were compared in a concentration-dependent manner. The results depict that GC ZnO-NPs exhibited greater inhibition compared to UC ZnO-NPs. This suggests that the degradation of biological activity is most likely due to the agglomeration of the uncapped nanoparticles in the latter case [86]. The superior inhibitory potential of GC ZnO-NPs compared to metformin indicates their effectiveness in controlling elevated blood glucose levels (Fig. 12, Table-3).

TABLE-3
α-AMYLASE INHIBITION ASSAY OF
ZnO NANOPARTICLES AND METFORMIN

Samples	IC_{50} (µg/mL)
GC ZnO-NPs	521 ± 0.004
UC ZnO-NPs	530 ± 0.010
Metformin	502 ± 0.010

*Data are IC_{50} ± SD (Standard deviation).

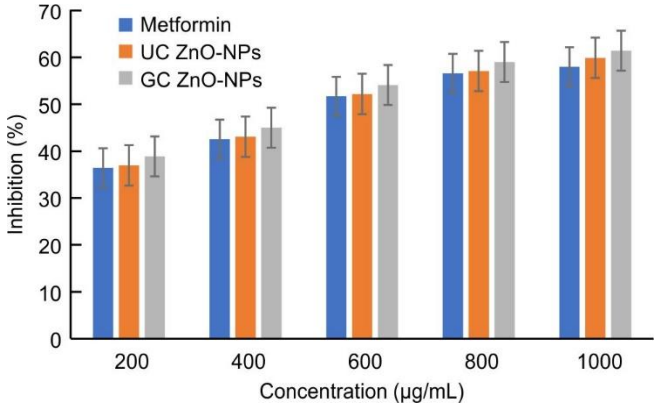

Fig. 12. α-Amylase inhibition assay of ZnO nanoparticles and metformin

Conclusion

The structure-activity relationship studies demonstrate the interaction of plant-derived bioactive compounds with dicarbonyl species (*e.g.* methylglyoxal), reflecting their antidiabetic properties. The integration of these bioactive compounds into nanotechnology improves their efficacy and stability, contributing to the formation of nanoparticles that may act as future drug candidates. The present work highlights green synthesis of ZnO nanoparticles by modifying their surface with a biocompatible capping agent (glucose) for the first time. The study demonstrated the efficacy of aqueous leaf extract of *S. nigrum* as a reducing agent and glucose as a capping and stabilizing agent. Various characterization techniques were employed to highlight the unique properties of the synthesized ZnO NPs. The study reports that ZnO NPs exhibited better antioxidant activity and *in vitro* α-amylase activity, supporting their potential as future antidiabetic agents. However, *in vivo* studies using appropriate diabetic models are important to investigate underlying mechanistic pathways, like inhibition of AGEs, antioxidant defense mechanisms and others, to establish a deeper understanding of the therapeutic roles of these ZnO NPs. The high IC_{50} values against metformin suggest that their efficacy in clinical settings may remain modest unless further optimized. A major limitation is the unassessed cytotoxicity of the nanoparticles, while moderate zeta potential suggests potential instability in biological environments. Still, with optimization, these biogenic nanoparticles hold promise as biocompatible agents for targeted drug delivery.

ACKNOWLEDGEMENTS

The authors are grateful to Prof. Abbas Ali Mahdi, Vice Chancellor and Pro-Vice Chancellor Prof. Farzana Mahedi, Era University, Lucknow, India, for providing the analytical and laboratory facilities. The authors are also grateful to the Birbal Sahni Institute of Palaeosciences (BSIP), Lucknow, the National Institute of Pharmaceutical Education and Research (NIPER), Raebareli, the Indian Institute of Toxicology Research (IITR), Lucknow and the Indian Institute of Technology (BHU), Varanasi, for providing analytical facilities.

CONFLICT OF INTEREST

The authors declare that there is no conflict of interests regarding the publication of this article.

REFERENCES

1. T.A. Debele and Y. Park, *Life*, **12**, 2078 (2022); https://doi.org/10.3390/life12122078
2. P.M. Mazumder, P. Rathinavelusamy and D. Sasmal, *Asian Pac. J. Trop. Dis.*, **2**, S969 (2012); https://doi.org/10.1016/S2222-1808(12)60303-X
3. International Diabetes Federation Diabetes Atlas, https://idf.org/
4. N.H. Cho, J.E. Shaw, S. Karuranga, Y. Huang, J.D. Da Rocha Fernandes, A.W. Ohlrogge and B. Malanda, *Diabetes Res. Clin. Pract.*, **138**, 271 (2018); https://doi.org/10.1016/j.diabres.2018.02.023
5. Diabetes, https://www.who.int/news-room/fact-sheets/detail/diabetes
6. Y. Chen, Z. Meng, Y. Li, S. Liu, P. Hu and E. Luo, *Mol. Med.*, **30**, 141 (2024); https://doi.org/10.1186/s10020-024-00905-9
7. A. Talwar, N. Chakraborty, M. Zahera, S. Anand, I. Ahmad, S. Siddiqui, A. Nayyar, A. Haque and M. Saeed, *J. Chem.*, **2024**, 6111603 (2024); https://doi.org/10.1155/2024/6111603
8. G. Boden, C. Homko, C.A. Barrero, T.P. Stein, X. Chen, P. Cheung, C. Fecchio, S. Koller and S. Merali, *Sci. Transl. Med.*, **7**, 304re7 (2015); https://doi.org/10.1126/scitranslmed.aac4765
9. A. Tentolouris, P. Vlachakis, E. Tzeravini, I. Eleftheriadou and N. Tentolouris, *Int. J. Environ. Res. Public Health*, **16**, 2965 (2019); https://doi.org/10.3390/ijerph16162965
10. F. Zannad, J.P. Ferreira, S.J. Pocock, S.D. Anker, J. Butler, G. Filippatos, M. Brueckmann, A.P. Ofstad, E. Pfarr, W. Jamal and M. Packer, *Lancet*, **396**, 819 (2020); https://doi.org/10.1016/S0140-6736(20)31824-9
11. S. Mondal, N. Roy, R.A. Laskar, I. Sk, S. Basu, D. Mandal and N.A. Begum, *Colloids Surf. B Biointerfaces*, **82**, 497 (2011); https://doi.org/10.1016/j.colsurfb.2010.10.007
12. A. Samadder, *World J. Transl. Med.*, **3**, 84 (2014); https://doi.org/10.5528/wjtm.v3.i2.84
13. M.A. Hassaan, *Int. J. Atmospheric Ocean. Sci.*, **2**, 10 (2018); https://doi.org/10.11648/j.ijaos.20180201.12
14. C. Hano and B.H. Abbasi, *Biomolecules*, **12**, 31 (2021); https://doi.org/10.3390/biom12010031
15. H. Bar, D. Bhui, G.P. Sahoo, P. Sarkar, S.P. De and A. Misra, *Colloids Surf. A Physicochem. Eng. Asp.*, **339**, 134 (2009); https://doi.org/10.1016/j.colsurfa.2009.02.008
16. G. Saibu and O. Adu, *J. Res. Rev. Sci.*, **7**, (2020); https://doi.org/10.36108/jrrslasu/0202.70.0120
17. N. Asif, M. Amir and T. Fatma, *Bioprocess Biosyst. Eng.*, **46**, 1377 (2023); https://doi.org/10.1007/s00449-023-02886-1
18. V. Souza, C. Rodrigues, S. Valente, C. Pimenta, J. Pires, M. Alves, C. Santos, I. Coelhoso and A. Fernando, *Coatings*, **10**, 110 (2020); https://doi.org/10.3390/coatings10020110
19. M.Y. Al-darwesh, S.S. Ibrahim and M.A. Mohammed, *Results Chem.*, **7**, 101368 (2024); https://doi.org/10.1016/j.rechem.2024.101368
20. J. Jansen, W. Karges and L. Rink, *J. Nutr. Biochem.*, **20**, 399 (2009); https://doi.org/10.1016/j.jnutbio.2009.01.009
21. G. Rehman, M. Umar, N. Shah, M. Hamayun, A. Ali, W. Khan, A. Khan, S. Ahmad, A.F. Alrefaei, M.H. Almutairi, Y.-S. Moon and S. Ali, *Pharmaceuticals*, **16**, 1677 (2023); https://doi.org/10.3390/ph16121677
22. N.A.N. Mohamad, N.A. Arham, J. Jai and A. Hadi, *Adv. Mat. Res.*, **832**, 350 (2013); https://doi.org/10.4028/www.scientific.net/AMR.832.350
23. A. Kanchana, S. Devarajan and S.R. Ayyappan, *Nano-Micro Lett.*, **2**, 169 (2010); https://doi.org/10.1007/BF03353637
24. V.V. Makarov, A.J. Love, O.V. Sinitsyna, S.S. Makarova, I.V. Yaminsky, M.E. Taliansky and N.O. Kalinina, *Acta Nat.*, **6**, 35 (2014); https://doi.org/10.32607/20758251-2014-6-1-35-44
25. S. Kheirouri, M. Alizadeh and V. Maleki, *Clin. Exp. Pharmacol. Physiol.*, **45**, 491 (2018); https://doi.org/10.1111/1440-1681.12904
26. R.A. Sperling and W.J. Parak, *Philos. Trans.- Royal Soc., Math. Phys. Eng. Sci.*, **368**, 1333 (2010); https://doi.org/10.1098/rsta.2009.0273
27. S. Svenson and R.K. Prud'homme, Multifunctional Nanoparticles for Drug Delivery Applications: Imaging, Targeting, and Delivery; Nanostructure Science and Technology; Springer US: Boston, MA (2012).
28. A. Banerjee, N. Dasgupta and B. De, *Food Chem.*, **90**, 727 (2005); https://doi.org/10.1016/j.foodchem.2004.04.033
29. H.M. Abdelmigid, N.A. Hussien, A.A. Alyamani, M.M. Morsi, N.M. AlSufyani and H.A. Kadi, *Molecules*, **27**, 1236 (2022); https://doi.org/10.3390/molecules27041236
30. M.A. Armani, A. Abu-Taleb, N. Remalli, M. Abdullah, V.V.S.S. Srikanth and N.K. Labhasetwar, *RSC Adv.*, **6**, 44145 (2016); https://doi.org/10.1039/C6RA05061A
31. N. Bahari, N. Hashim, K. Abdan, A. Md Akim, B. Maringgal and L. Al-Shdifat, *Nanomaterials*, **13**, 1244 (2023); https://doi.org/10.3390/nano13071244
32. R. Javed, M. Zia, S. Naz, S.O. Aisida, N.U. Ain and Q. Ao, *J. Nanobiotechnology*, **18**, 172 (2020); https://doi.org/10.1186/s12951-020-00704-4
33. S. Gulati, M. Sachdeva and K.K. Bhasin, *AIP Conf. Proc.*, **1953**, 030214 (2018); https://doi.org/10.1063/1.5032549
34. G. Brancolini, V.M. Rotello and S. Corni, *Int. J. Mol. Sci.*, **23**, 2368 (2022); https://doi.org/10.3390/ijms23042368
35. Z. Bahadoran, P. Mirmiran and F. Azizi, *J. Diabetes Metab. Disord.*, **12**, 43 (2013); https://doi.org/10.1186/2251-6581-12-43
36. S. Yagihashi, H. Mizukami and K. Sugimoto, *J. Diabetes Investig.*, **2**, 18 (2011); https://doi.org/10.1111/j.2040-1124.2010.00070.x
37. Q. Kang and C. Yang, *Redox Biol.*, **37**, 101799 (2020); https://doi.org/10.1016/j.redox.2020.101799
38. K. Gąsiorowski, B. Brokos, V. Echeverria, G.E. Barreto and J. Leszek, *Mol. Neurobiol.*, **55**, 1463 (2018); https://doi.org/10.1007/s12035-017-0419-4
39. P.J. Thornalley, A. Langborg and H.S. Minhas, *Biochem. J.*, **344**, 109 (1999); https://doi.org/10.1042/bj3440109
40. A. Parveen, R. Sultana, S.M. Lee, T.H. Kim and S.Y. Kim, *Arch. Pharm. Res.*, **44**, 378 (2021); https://doi.org/10.1007/s12272-021-01323-9
41. D. Bhuyan, B. Malakar, S.S. Arbuj and L. Saikia, *RSC Adv.*, **4**, 8256 (2014); https://doi.org/10.1039/c3ra45818k
42. E. Darvishi, D. Kahrizi and E. Arkan, *J. Mol. Liq.*, **286**, 110831 (2019); https://doi.org/10.1016/j.molliq.2019.04.108
43. B. Bulcha, J. Leta Tesfaye, D. Anatol, R. Shanmugam, L.P. Dwarampudi, N. Nagaprasad, V. Bhargavi and R. Krishnaraj, *J. Nanomater.*, **2021**, 8617290 (2021); https://doi.org/10.1155/2021/8617290
44. S. Gopalakrishnan and P. Kolandaivel, *Mater. Chem. Phys.*, **181**, 248 (2016); https://doi.org/10.1016/j.matchemphys.2016.06.056
45. G. Patwari, P.K. Kalita and R. Singha, *Mater. Sci. Pol.*, **34**, 69 (2016); https://doi.org/10.1515/msp-2016-0030
46. W.J. Jeyarani, T. Tenkyong, N. Bachan, D.A. Kumar and J.M. Shyla, *Adv. Powder Technol.*, **27**, 338 (2016); https://doi.org/10.1016/j.apt.2016.01.006
47. A. Goudarzi, E. Zabihi, D. Shahrampour and M. Heydari Sorshejani, *J. Mater. Sci. Mater. Electron.*, **33**, 22798 (2022); https://doi.org/10.1007/s10854-022-09047-2
48. P.V. Gaikwad, P.K. Pujari and A. Kshirsagar, *ACS Omega*, **3**, 7692 (2018); https://doi.org/10.1021/acsomega.8b00998
49. S.B. Rana, V.K. Bhardwaj, S. Singh, A. Singh and N. Kaur, *J. Exp. Nanosci.*, **9**, 877 (2014); https://doi.org/10.1080/17458080.2012.736640
50. C.-W. Chen, K.-H. Chen, C.-H. Shen, A. Ganguly, L.-C. Chen, J.-J. Wu, H.-I. Wen and W.-F. Pong, *Appl. Phys. Lett.*, **88**, 241905 (2006); https://doi.org/10.1063/1.2211047
51. N. Govindan, K. Vairaprakasam, C. Chinnasamy, T. Sivalingam and M.K.A. Mohammed, *Mater. Adv.*, **1**, 3460 (2020); https://doi.org/10.1039/D0MA00698J

52. D. Lilhare and A. Khare, *Mater. Chem. Phys.*, **270**, 124835 (2021); https://doi.org/10.1016/j.matchemphys.2021.124835
53. B. Naiel, M. Fawzy, M.W.A. Halmy and A.E.D. Mahmoud, *Sci. Rep.*, **12**, 20370 (2022); https://doi.org/10.1038/s41598-022-24805-2
54. A.A. Barzinjy and H.H. Azeez, *SN Appl. Sci.*, **2**, 991 (2020); https://doi.org/10.1007/s42452-020-2813-1
55. R.M.I. Elsamra, M.S. Masoud, A.A. Zidan, G.M.E. Zokm and M.A. Okbah, *Biomass Convers. Biorefin.*, **14**, 16843 (2024); https://doi.org/10.1007/s13399-022-03709-1
56. E.F. El-Belely, M.M.S. Farag, H.A. Said, A.S. Amin, E. Azab, A.A. Gobouri and A. Fouda, *Nanomaterials*, **11**, 95 (2021); https://doi.org/10.3390/nano11010095
57. S. Vijayakumar, S. Mahadevan, P. Arulmozhi, S. Sriram and P.K. Praseetha, *Mater. Sci. Semicond. Process.*, **82**, 39 (2018); https://doi.org/10.1016/j.mssp.2018.03.017
58. P.A. Wiguna, N. Yudasari, D. Djuhana and C. Imawan, *J. Phys.: Conf. Ser.*, **1317**, 012061 (2018); https://doi.org/10.1088/1742-6596/1317/1/012061
59. R. Sattari, G.R. Khayati and R. Hoshyar, *Mater. Chem. Phys.*, **241**, 122438 (2020); https://doi.org/10.1016/j.matchemphys.2019.122438
60. K. Vimala, S. Sundarraj, M. Paulpandi, S. Vengatesan and S. Kannan, *Process Biochem.*, **49**, 160 (2014); https://doi.org/10.1016/j.procbio.2013.10.007
61. E. Tomaszewska, K. Soliwoda, K. Kadziola, B. Tkacz-Szczesna, G. Celichowski, M. Cichomski, W. Szmaja and J. Grobelny, *J. Nanomater.*, **2013**, 313081 (2013); https://doi.org/10.1155/2013/313081
62. S.K. Filippov, R. Khusnutdinov, A. Murmiliuk, L.Ya. Zakharova, W. Inam, H. Zhang and V.V. Khutoryanskiy, *Mater. Horiz.*, **10**, 5354 (2023); https://doi.org/10.1039/D3MH00717K
63. X. Wang, O. Ramström and M. Yan, *Analyst*, **136**, 4174 (2011); https://doi.org/10.1039/c1an15469a
64. F. Kalhori, H. Yazdyani, F. Khademorezaeian, N. Hamzkanloo, P. Mokaberi, S. Hosseini and J. Chamani, *Luminescence*, **37**, 1836 (2022); https://doi.org/10.1002/bio.4360
65. H.M.H. Al-Kordy, S.A. Sabry and M.E.M. Mabrouk, *Sci. Rep.*, **11**, 10924 (2021); https://doi.org/10.1038/s41598-021-90408-y
66. B.D. Lakshmi, B.V. Vamsi Krishna, P.T. Rao, A. Marukurti, V. K, E.B. Sk and K.R. Rao, *ACS Omega*, **9**, 38396 (2024); https://doi.org/10.1021/acsomega.4c01727
67. Z. Lukáčová Bujňáková, E. Dutková, J. Jakubíková, D. Cholujová, R. Varhač, L. Borysenko and I. Melnyk, *Pharmaceuticals*, **16**, 1219 (2023); https://doi.org/10.3390/ph16091219
68. A.K. Sidhu, N. Verma and P. Kaushal, *Front. Nanotechnol.*, **3**, 801620 (2022); https://doi.org/10.3389/fnano.2021.801620
69. A. Fouda, E. Saied, A.M. Eid, F. Kouadri, A.M. Alemam, M.F. Hamza, M. Alharbi, A. Elkelish and S.E.-D. Hassan, *J. Funct. Biomater.*, **14**, 205 (2023); https://doi.org/10.3390/jfb14040205.
70. A. Aldalbahi, S. Alterary, R.A.A. Almoghim, M.A. Awad, N.S. Aldosari, S.F. Alghannam, A.N. Alabdan, S. Alharbi, B.A.M. Alateeq, A.A. Al Mohsen, M.A. Alkathiri and R.A. Alrashed, *Molecules*, **25**, 4198 (2020); https://doi.org/10.3390/molecules25184198
71. M. Danaei, M. Dehghankhold, S. Ataei, F.H. Davarani, R. Javanmard, A. Dokhani, S. Khorasani and M.R. Mozafari, *Pharmaceutics*, **10**, 57 (2018); https://doi.org/10.3390/pharmaceutics10020057
72. M. Ramesh, M. Anbuvannan and G. Viruthagiri, *Spectrochim. Acta A Mol. Biomol. Spectrosc.*, **136**, 864 (2015); https://doi.org/10.1016/j.saa.2014.09.105
73. U.L. Ifeanyichukwu, O.E. Fayemi and C.N. Ateba, *Molecules*, **25**, 4521 (2020); https://doi.org/10.3390/molecules25194521
74. R. Sathyavathi, M.B. Krishna, S.V. Rao, R. Saritha and D.N. Rao, *Adv. Sci. Lett.*, **3**, 138 (2010); https://doi.org/10.1166/asl.2010.1099
75. S.K.K. Supin, P.N.P.M. Parvathy and M. Vasundhara, *RSC Adv.*, **13**, 1497 (2023); https://doi.org/10.1039/D2RA06967A
76. S.S. Sana, D.V. Kumbhakar, A. Pasha, S.C. Pawar, A.N. Grace, R.P. Singh, V.-H. Nguyen, Q.V. Le and W. Peng, *Molecules*, **25**, 4896 (2020); https://doi.org/10.3390/molecules25214896
77. M.D. Jayappa, C.K. Ramaiah, M.A.P. Kumar, D. Suresh, A. Prabhu, R.P. Devasya and S. Sheikh, *Appl. Nanosci.*, **10**, 3057 (2020); https://doi.org/10.1007/s13204-020-01382-2
78. P. Wongsa, P. Phatikulrungsun and S.F.T.-I.R. Prathumthong, *Sci. Rep.*, **12**, 6631 (2022); https://doi.org/10.1038/s41598-022-10669-z
79. K.B. Ishnava, J.B. Chauhan and M.B. Barad, *Saudi J. Biol. Sci.*, **20**, 69 (2013); https://doi.org/10.1016/j.sjbs.2012.11.003
80. D.K. Buslov, N.A. Nikonenko, N.I. Sushko and R.G. Zhbankov, *Spectrochim. Acta A Mol. Biomol. Spectrosc.*, **55**, 229 (1998); https://doi.org/10.1016/S1386-1425(98)00289-3
81. P. Rajiv, S. Rajeshwari and R. Venckatesh, *Spectrochim. Acta A Mol. Biomol. Spectrosc.*, **112**, 384 (2013); https://doi.org/10.1016/j.saa.2013.04.072
82. E.P. Etape, J. Foba-Tendo, L.J. Ngolui, B.V. Namondo, F.C. Yollande and M.B.N. Nguimezong, *J. Nanomater.*, **2018**, 1 (2018); https://doi.org/10.1155/2018/9072325
83. A. Jayachandran, A. T.R and A.S. Nair, *Biochem. Biophys. Rep.*, **26**, 100995 (2021); https://doi.org/10.1016/j.bbrep.2021.100995
84. A. Campisi, R. Acquaviva, G. Raciti, A. Duro, M. Rizzo and N.A. Santagati, *Foods*, **8**, 63 (2019); https://doi.org/10.3390/foods8020063
85. A.K. Tiwari, S. Jha, S.K. Tripathi, R. Shukla, R.R. Awasthi, A.K. Bhardwaj, A.K. Singh and A. Dikshit, *Discov. Appl. Sci.*, **6**, 399 (2024); https://doi.org/10.1007/s42452-024-06049-z
86. Y. Song, F. Yang, M. Ma, Y. Kang, A. Hui, Z. Quan and A. Wang, *Lebensm. Wiss. Technol.*, **165**, 113762 (2022); https://doi.org/10.1016/j.lwt.2022.113762